Bulletin of the Seismological Society of America, Vol. 92, No. 5, pp. 1841–1846, June 2002

A Bilinear Source-Scaling Model for **M**–log *A* Observations of Continental Earthquakes

by Thomas C. Hanks and William H. Bakun

Abstract The Wells and Coppersmith (1994) **M**–log *A* data set for continental earthquakes (where **M** is moment magnitude and *A* is fault area) and the regression lines derived from it are widely used in seismic hazard analysis for estimating **M**, given *A*. Their relations are well determined, whether for the full data set of all mechanism types or for the subset of strike-slip earthquakes. Because the coefficient of the log *A* term is essentially 1 in both their relations, they are equivalent to constant stress-drop scaling, at least for $\mathbf{M} \leq 7$, where most of the data lie. For $\mathbf{M} > 7$, however, both relations increasingly underestimate the observations with increasing **M**. This feature, at least for strike-slip earthquakes, is strongly suggestive of L-model scaling at large **M**. Using constant stress-drop scaling ($\Delta\sigma = 26.7$ bars) for $\mathbf{M} \leq 6.63$ and L-model scaling (average fault slip $\bar{u} = \alpha L$, where L is fault length and $\alpha = 2.19$ &times 10^{-5}) at larger **M**, we obtain the relations

$$\mathbf{M} = \log A + 3.98 \pm 0.03, \; A \leq 537 \text{ km}^2$$

and

$$\mathbf{M} = 4/3 \log A + 3.07 \pm 0.04, \; A > 537 \text{ km}^2.$$

These prediction equations of our bilinear model fit the Wells and Coppersmith (1994) data set well in their respective ranges of validity, the transition magnitude corresponding to $A = 537$ km^2 being $\mathbf{M} = 6.71$.

Introduction

The moment magnitude (**M**)–fault area (*A*) relations of Wells and Coppersmith (1994), hereafter WC94, are used in seismic hazard analyses throughout the world because of the common practice of estimating earthquake size from observations or inferences of fault length (*L*) and fault width (*W*), of which *A* is the product. These relations are

$$\mathbf{M} = (0.98 \pm 0.03) \log A + (4.07 \pm 0.06), \quad (1)$$

the regression line for 148 earthquakes of all mechanism types (strike-slip, reverse, and normal; Table 2A and Figure 16a of WC94); and

$$\mathbf{M} = (1.02 \pm 0.03) \log A + (3.98 \pm 0.07), \quad (2)$$

the regression line for 83 strike-slip earthquakes (Table 2A of WC94), where *A* has units of km^2. The regression lines (1) and (2) are well determined, as indicated by the small standard errors (± 1 sigma) for the regression coefficients, and they are essentially identical to the model constant stress-drop (30 bars) relationship $\mathbf{M} = \log A + 4.03$ we develop below.

In both cases, however, these regression lines slightly, but noticeably, underestimate **M**, for a given *A*, at $\mathbf{M} \gtrsim 7$, as is evident from Figure 16a of WC94 and Figure 1 here. Systematically underestimating **M** for large earthquakes by just 0.2 units is equivalent to underestimating seismic moment by a factor of 2, if seismic moments are determined from these biased estimates of **M**. For seismic hazard analyses constrained by the balance of elastic strain energy accumulated through plate motions and released through earthquakes, generally reckoned in terms of seismic moment sums, such biased estimates of seismic moments will result in more numerous, smaller-magnitude earthquakes. This in turn will lead to correspondingly—and erroneously—higher mean annual rates of occurrence for $\mathbf{M} \gtrsim 7$ earthquakes, the magnitude range affected by the systematic bias.

Equations (1) and (2) arise from the massive database compiled in WC94, fault-rupture data for 244 continental, crustal (depth < 40 km) earthquakes of all mechanism types in both interplate and intraplate settings. These data include

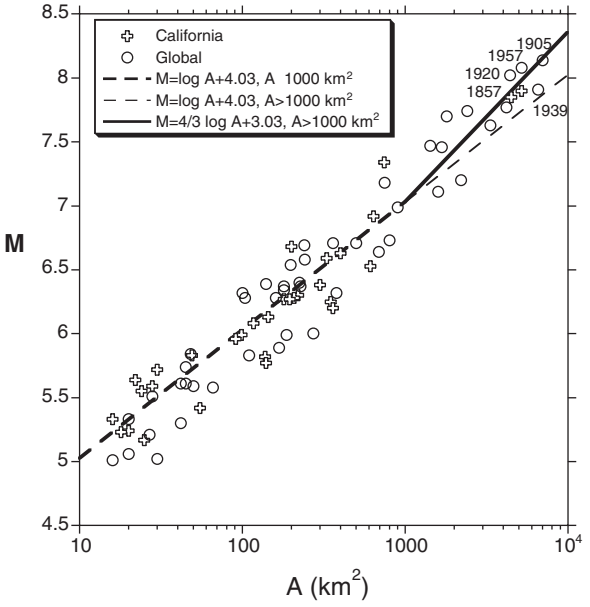

Figure 1. Model equations (7) and (13) and WC94 **M**–log *A* data for continental strike-slip earthquakes. Unlabeled symbols denote 75 **M** ≥5.0 continental, strike-slip earthquakes that qualified for the WC94 regression analysis (see text). The labeled (by year of occurrence) symbols denote five additional **M** ≥7.5, continental, strike-slip earthquakes with **M**–log *A* data given in Table 1.

seismic moment, moment magnitude, rupture length, rupture width, rupture area, and rupture displacements for each event. A data set of this scope and size is not without limitations, naturally. That only 148 of the possible 244 earthquakes were used in the WC94 regression relationship is testimony to the uncertainty residing in this data set, much of it attending earthquakes occurring at early dates or in remote places (or both). In the modern era, yet another problem arises in the multiplicity of often inconsistent estimates for these fault-rupture parameters, as they might be obtained from geologic field observations, aftershock locations, geodetic inversions, and waveform analysis (at local, regional, and teleseismic distances). Finally, the continental-crust criterion of WC94 excludes earthquakes at subduction zones, both those at the interface and those within the downgoing slab, and thus excludes the world's truly great earthquakes. These caveats notwithstanding, we know of no data set that is better for the many purposes this one serves, and the systematics of the WC94 data set are impressive, as is their concordance with the simple source-scaling relationships we will present in this article, both above and below **M** = 7 (Fig. 1).

The bulk of this article is devoted to the development of **M**–log *A* relations that span the transition from small earthquakes with circular geometry to large earthquakes with rectangular geometry. This transition should be better expressed for strike-slip earthquakes, because fault width *W* can be much larger for the largest thrust-faulting earthquakes than for the largest strike-slip earthquakes. Thus, the data we explore here is the strike-slip subset of the full WC94 data set. Given the restriction to continental earthquakes, the strike-slip subset contains all but one of the earthquakes with **M** ≥ 7.5. It is worth noting, however, that neither the **M**–log *A* data themselves (WC94 Fig. 16a) nor the empirical relations developed separately for strike-slip, reverse, or normal faulting earthquakes (WC94 Fig. 16b and Table 2A) allow any distinction to be made between these mechanism types.

Figure 1 shows the 83 continental strike-slip earthquakes in the WC94 data set that qualified for their regression analysis, less 8 earthquakes with **M** < 5. In this context "qualifying" means that the estimates of **M**, *L*, and *W* (and thus *A*) are well determined. We have also included in Figure 1 five additional great continental, strike-slip earthquakes, identified by their year of occurrence, which doubles the data set at **M** ≥ 7.5. These are the 1857 Fort Tejon, California; 1905 Bulnay, Mongolia; 1920 Haiyuan, China; 1939 Erzincan, Turkey; and 1957 Gobi-Altay, Mongolia earthquakes. They are plotted with the **M** and *A* data shown in Table 1.

These five earthquakes did not qualify for the WC94 regression analysis, because of uncertainties in **M**, *L*, or *W*, primarily in *W*, but much new data for these earthquakes have recently become available. Even so, the values of *W* are basically assumed, although we have tended toward the larger possible values—which, as we shall see shortly, push the data toward the WC94 regression lines and away from the model we prefer.

Small Earthquake Scaling

We begin with the circular-fault, r^3-scaling appropriate to small earthquakes with dimension $2r \leq W_s$, the seismogenic width (or depth) of the continental crust:

$$M_0 = 16/7\Delta\sigma r^3, \tag{3}$$

where M_0 is seismic moment, $\Delta\sigma$ is the earthquake stress drop, and r is the radius of the circular crack (Brune, 1971). For $A = \pi r^2$,

$$\log M_0 = 3/2 \log A + \log\Delta\sigma - 0.387, \tag{4}$$

Moment magnitude (Hanks and Kanamori, 1979) is

$$\mathbf{M} \equiv 2/3 \log M_0 - 10.7. \tag{5}$$

Substituting equation (4) into (5) yields

$$\mathbf{M} = \log A + 2/3 \log\Delta\sigma - 10.958. \tag{6}$$

Finally, for an average earthquake stress drop of 30 bars (3×10^7 dyne/cm^2) (e.g., Aki, 1972; Thatcher and Hanks,

Table 1
Supplemental **M** ≥7.5 Earthquakes

Date	Name	Length L (km)	Width W (km)*	Area A (km^2)	u (m)	μ (10^{11} dyne/cm^2)	M_0 (10^{28} dyne-cm)	**M**	Sources
1857	Fort Tejon, California	300	15	4500	5	3.00	0.68†	7.85	Sieh (1978); Stein and Hanks (1998)
1905	Bulnay, Mongolia	350	20	7000	8	3.30	1.85†	8.14	D.P. Schwartz (personal commun., 2001)
1920	Haiyuan, China	220	20	4400	8.3	3.30	1.2‡	8.02	Chen and Molnar (1977); Zhang *et al.* (1987)
1939	Erzincan, Turkey	327	20	6540	4	3.15	0.82†	7.91	Stein *et al.* (1997)
1957	Gobi-Altay, Mongolia	260	20	5200	4	3.30	1.5‡	8.08	Okal (1976); Chen and Molnar (1977); Kurushin *et al.* (1997); D. P. Schwartz (personal commun., 2001)

*Assumed values.
†Derived from $M_0 = \mu u A$, where $A = LW$.
‡Derived from seismic data.

1973; Kanamori and Anderson, 1975; Hanks, 1977) and with $\log A$ (cm^2) = 10.0 + $\log A$ (km^2), the units of WC94,

$$\mathbf{M} = \log A + 4.03. \quad (7)$$

The retention of three significant figures in the intercept value of equation (7) seems excessive, but it is necessary for the accurate estimation of seismic moment that modern seismic hazard analyses now require.

Equation (7) is shown in Figure 1 as the dashed line. Up to about $\mathbf{M} = 7$ and $A = 1000$ km^2, equation (7) is a surprisingly good match to the data, given the very simple model construct. For $5 \leq \mathbf{M} \leq 7$, the regression lines (1) and (2) differ from equation (7) by no more than 0.03 units in **M**, about the thickness of the dashed line. At larger **M** and A, however, the data trend systematically away from and above equation (7)—which is true for equations (1) and (2) as well.

Large Earthquake Scaling

The mismatch of data and models at $A > 1000$ km^2 and $\mathbf{M} > 7$ suggests that an increasing stress drop sets in beyond these values of A and **M**, about where we expect the transition from $A = \pi r^2$ geometry at small magnitude to the $A = LW$ geometry at large magnitude to occur, at least for continental strike-slip earthquakes. One way to achieve this appearance of increasing stress drop is through L-model scaling, for which the average faulting displacement $\bar{u}$ increases with L. Conversely, W-model scaling provides for $\bar{u}$ to saturate with $W = W_s$, no matter how much larger L might be than W.

The arguments for and against L-model scaling vis-à-vis W-model scaling have ebbed and flowed for two decades now (e.g., Scholz, 1982; Scholz *et al.*, 1986; Romanowicz, 1992, 1994; Romanowicz and Rundle, 1993; Scholz, 1994a,b; 1997). Most of this controversy preceded publication of WC94, but to our knowledge the WC94 data set has never been brought to bear on the important matters of *L-affaire*, so to speak.

For the rectangular faults associated with large, continental strike-slip earthquakes,

$$M_0 = \mu \bar{u} LW, \quad (8)$$

where μ is the shear modulus and $A = LW$. For W-model scaling, $\bar{u}$ is constant with increasing L and fixed $W = W_s$. Then, because of the moment–magnitude relation (5), **M** ~2/3 log A, which makes matters worse, not better, in matching data above the constant stress-drop line $\mathbf{M} = \log A + 4.03$.

The L-model scaling possibilities are more promising. Indeed, the regression relation between $\bar{u}$ and L for strike-slip earthquakes found in Table 2C of WC94,

$$\log \bar{u} = (-1.70 \pm 0.23) + (1.04 \pm 0.13) \log L, \quad (9)$$

is by itself evidence for L-model scaling. Standard errors of the regression coefficients are again given as ±1 sigma, and it does not hurt much to set the coefficient of the log L term in equation (9) to 1.00, so to recover the first-order approximation

$$\bar{u} = \alpha L \quad (10)$$

upon inversion of the logarithmic form (9). This inversion yields $\alpha = 0.02$ m of average slip per 1 km of fault length, or 2×10^{-5}. Similarly, the logarithmic uncertainty in equation (9) means that the 1-sigma uncertainty of α in equation (10) is a factor of 1.7, permitting the range $1.2 \times 10^{-5} \leq \alpha \leq 3.4 \times 10^{-5}$.

Using equation (10) in equation (8), we have,

$$M_0 = \mu\alpha L^2 W = \mu\alpha A^2/W, \quad (11)$$

and using this in turn in the moment–magnitude relation (5) yields

$$\mathbf{M} = 4/3 \log A + 2/3 \log(\mu\alpha/W) - 10.7. \quad (12)$$

With the choices of $\mu = 3 \times 10^{11}$ dyne/cm^2, $\alpha = 2 \times 10^{-5}$, $W = W_s = 1.5 \times 10^6$ cm, and the area conversion to km^2,

$$\mathbf{M} = 4/3\log A + 3.03. \quad (13)$$

Equation (13) crosses equation (7) at $A = 1000$ km^2 and $\mathbf{M} = 7.00$, and we plot it in Figure 1 for A and $\mathbf{M}$ in excess of these values. Within its range of validity, it too is a very good match to the data, as is the constant stress-drop relation (7) at smaller magnitude.

Best-Fit Models

We calculate best fits of the data to equations (7) and (13) on the basis of leaving the log A coefficients as fixed by the source-scaling analysis but allowing the intercept values to be determined by a least-squares fit to the data. This procedure allows us to determine best estimates of $\Delta\sigma$ in equation (7) and α in equation (13). We performed this calculation in two steps. First, we operated on equation (7) with data $\mathbf{M} \leq 7.00$ and on equation (13) with the data at $\mathbf{M} > 7.00$. This round of calculations yielded an intercept value of 3.98 instead of the 4.03 in equation (7), a very modest change corresponding to a 12% reduction in $\Delta\sigma$ (that is, $\Delta\sigma = 26.7$ bars). For equation (13), the intercept value changed from 3.03 to 3.09, also a fairly modest change corresponding to a 15% increase in α, well within the permissible range. Because of the small difference in slope between these two lines, however, the crossover values change considerably, to $A = 467$ km^2 and $\mathbf{M} = 6.65$ from $A = 1000$ km^2 and $\mathbf{M} = 7.00$.

The second iteration was to adjust the intercept value of equation (13) using only data at $A \geq 467$ km^2 and $\mathbf{M} \geq 6.65$, without operating again on equation (7). This results in the following prediction equations, which we recommend to those who seek to estimate the size of shallow-focus, continental, strike-slip earthquakes given an estimate of A:

$$\mathbf{M} = \log A + 3.98 \pm 0.03, A \leq 537 \text{ km}^2 \quad (7a)$$

and

$$\mathbf{M} = 4/3\log A + 3.07 \pm 0.04, A > 537 \text{ km}^2. \quad (13a)$$

The uncertainty estimates are the 1-sigma uncertainties in the intercept values and show that the best-fit prediction equations (7a) and (13a) are not significantly different from the model equations (7) and (13).

The prediction equations (7a) and (13a) are shown in Figure 2a, which reproduces the data in Figure 1. The poor resolution in determining the crossover pair $A = 537$ km^2 and $\mathbf{M} = 6.71$ is unfortunate, in that it does not allow us to define well the dimensions at which the faulting-geometry transition occurs. For $A = 537$ km^2 and $W = 15$ km, the crossover L is 36 km, about $2W$, as would be expected from image-source solutions for vertical rectangular cracks in an elastic halfspace rupturing from the surface down to 15 km depth (Chinnery, 1963).

Figure 2b shows residuals of the data with respect to the WC94 relation, equation (2), and the bilinear model developed here, equations (7a) and (13a). For $A \leq 500$ km^2, the residuals for both models are evenly distributed about zero, indicating that both models fit the data equally well;

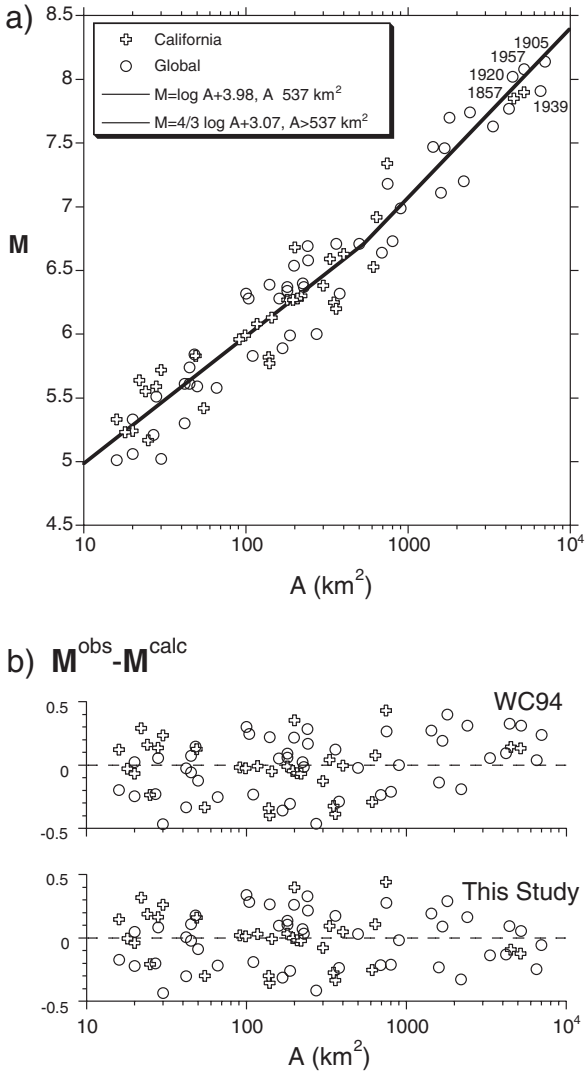

Figure 2. (a) Prediction equations (7a) and (13a), with data as in Fig. 1. (b) Magnitude residuals for the Wells and Coppersmith (1994) relation (equation 2) and the bilinear prediction equations proposed in this study (equations 7a and 13a).

as we have noted earlier, equations (2) and (7a) are in fact indistinguishable from one another for $A \leq 500$ km^2. For $A > 500$ km^2, the WC94 residuals take on an increasingly positive character, and for $A > 3000$ km^2 and $\mathbf{M} > 7.5$ are absolutely and entirely positive for the eight largest earthquakes. Residuals for the model proposed here, equations (7a) and (13a), show no trend for $A > 500$ km^2 and are relatively small for the eight largest earthquakes except for the 1939 earthquake.

To put the graphical display of Figure 2b on a more quantitative basis, we have computed the χ^2 (chi-squared) statistic ($\chi^2 = \Sigma\{[1/\sigma_i^2][\mathrm{M}_i^{\mathrm{obs}} - \mathrm{M}_i^{\mathrm{calc}}]\}$) for the several ranges of A described below. (We use $\sigma_i = \sigma = 0.22$, which includes contributions from uncertainty in the estimates of **M** and A, which are assumed to be independent. Separately, we have calculated the standard deviation of all of the residuals $\mathbf{M}_i^{\mathrm{obs}} - \mathbf{M}_i^{\mathrm{calc}}$, to be 0.225 for Figure 2b, top, and 0.214 for Figure 2b, bottom, in sensible agreement with the sigma of 0.22 estimated from data uncertainties alone.) For $A \leq 537$ km^2, χ^2 for equation (2) is 1.04 times that for equation (7a), the latter being a slightly but inconsequentially better fit than the former for events in this range of A. For $A \geq 537$ km^2, the difference in the misfits is greater: χ^2 is 25.2 for equation (2) and 19.0 for equation (13a) for the 20 strike-slip events in this range of A. Finally, for the eight largest events with $A \geq 3000$ km^2, χ^2 is 6.59 for equation (2) but just 2.90 for equation (13a).

Discussion

As new data become available and as old data are revisited, the model equations (7) and (13) and the prediction equations (7a) and (13a) can of course be expected to change, although there are certain aspects of both the data and the models that suggest a robustness to them. There is little that is new in the constant stress-drop equations (7) and (7a), for example. Even before the advent of moment magnitude, the log $M_0 \sim 3/2 \log A$ relationship in equation (4) was known to Kanamori and Anderson (1975) and Wyss (1979). These studies also recognized the magnitude–fault area dependencies in equations (6) and (7), but in the form of surface-wave magnitude $M_s \sim \log A$. That earthquake stress drops are a scale-invariant property of crustal earthquakes, although with considerable scatter, has also been known for decades, both as a static property (e.g., Aki, 1972; Thatcher and Hanks, 1973; Kanamori and Anderson, 1975; Hanks, 1977) and as a dynamic property (e.g., Hanks and McGuire, 1981; Boore, 1983; Fletcher *et al.*, 1984; Choy and Boatwright, 1995). Absolute values of stress drops returned from different scaling relations can differ by a factor of 2 or so, as can dynamic versus static stress drops returned from the same scaling model. Nevertheless, the average static stress drop of 30 bars or so (with a full-range scatter of several factors of 2) recovered for these shallow-focus, continental, strike-slip, $\mathbf{M} \leq 7$ earthquakes in or near plate-boundary settings is very much the expected result.

For $\mathbf{M} \gtrsim 7$, our application of L-model scaling is potentially more controversial, but the concordance of data and model for $\mathbf{M} \gtrsim 7$ in Figures 1 and 2 is impressive. Both this concordance and the empirical relation between $\bar{u}$ and L found by WC94 and reproduced here as equations (9) and (10) provide strong support for L-model scaling. The trend of the data for $\mathbf{M} \gtrsim 7$ and its agreement with L-model scaling apparent in Figures 1 and 2 should also be apparent as trends of stress drop increasing with **M** or M_0. In his Figure 4, Scholz (1982) shows that stress drop increases systematically for interplate strike-slip earthquakes from $\Delta\sigma \sim 10$ bars at $M_0 \sim 10^{26}$ dyne-cm ($\mathbf{M} \sim 6.6$) to $\Delta\sigma \sim 100$ bars at $M_0 \sim 10^{28}$ dyne-cm ($\mathbf{M} \sim 8$). For thrust-faulting earthquakes, this trend occurs at much larger magnitude, because W can be so much greater for the largest thrust-faulting earthquakes than for the largest strike-slip earthquakes. The data, notably, are not the same: only 5 of the 14 strike-slip earthquakes found in Table 1 and Figure 4 of Scholz (1982) qualified for the regression analysis of WC94. Together with the 1857 and 1939 earthquakes, 7 of these 14 earthquakes are presented in Figures 1 and 2, but only 4 of these have $\mathbf{M} > 6.71$, our crossover magnitude.

L-model scaling does, however, have important implications for the different ways in which earthquakes must work above and below the transition magnitude, as recently discussed by Kanamori and Heaton (2000). Very recently, Shaw and Scholz (2001) have suggested, on the basis of both $\bar{u}$–L observations and synthetic $\bar{u}$–L data produced by three-dimensional dynamic rupture models, that L-model scaling works only up to an aspect ratio (L/W) of approximately 10. For $L/W \gtrsim 10$, the average faulting displacement no longer increases with fault length. We do not see this here, although our data set (**M**–log A) and theirs ($\bar{u}$–L) are not directly comparable, even though our model estimates at large **M** do incorporate L-model scaling (equation 10). Even more puzzling in this context are the results of Atkinson and Silva (1997) that the dynamic stress differences governing the excitation of high-frequency strong ground motion decrease with increasing magnitude above $\mathbf{M} = 5.5$. The unusually low amplitudes of high-frequency strong ground motion for the recent Izmit, Turkey (17 August 1999; $\mathbf{M} = 7.4$), and Chi-Chi, Taiwan (21 September 1999; $\mathbf{M} = 7.6$), earthquakes are also consistent with the findings of Atkinson and Silva (1997).

However these issues—so important to knowing the inner workings of crustal earthquakes—may be resolved, our bilinear model equations (7) and (13) and prediction equations (7a) and (13a) fit the WC94 continental, strike-slip earthquake **M**–log A data without bias—but not without the uncertainty arising from the natural variability in earthquake data of this sort. The prediction equations work equally well for the reverse- and normal-faulting earthquakes of WC94. In the case of equations (13 and 13a), the test is not strong, because only one of these non-strike-slip earthquakes has $\mathbf{M} \geq 7.5$. It does suggest, however, a limit for W of 20 km or so for such earthquakes in the continents, unlike the case

for the great subduction earthquakes in oceanic environments, for which W can be much larger.

Acknowledgments

D.L. Wells graciously provided us with the WC94 **M**–log A dataset in digital form. We appreciate the thoughtful commentary of D.J. Andrews, M.L. Blanpied, J.L. Boatwright, W. Foxall, and R.S. Stein who reviewed this manuscript in its early stages and of J.-R. Grasso and an anonymous reviewer who reviewed it for the *Bulletin*.

References

Aki, K. (1972). Earthquake mechanism, *Tectonophysics* **13,** 423–446.

Atkinson, G. M., and W. Silva (1997). An empirical study of earthquake source spectra for California earthquakes, *Bull. Seism. Soc. Am.* **87,** 97–113.

Brune, J. N. (1971). Correction, *J. Geophys. Res.* **76,** 5002.

Boore, D. M. (1983). Stochastic simulation of high-frequency ground motions based on seismological models of the radiated spectra, *Bull. Seism. Soc. Am.* **73,** 1865–1894.

Chen, W. P., and P. Molnar (1977). Seismic moments of major earthquakes and average rate of slip in central Asia, *J. Geophys. Res.* **82,** 2954–2969.

Chinnery, M. A. (1963). The stress changes that accompany strike-slip faulting, *Bull. Seism. Soc. Am.* **53,** 921–932.

Choy, G. L., and J. L. Boatwright (1995). Global patterns of radiated seismic energy and apparent stress, *J. Geophys. Res.* **100,** 18,205–18,228.

Fletcher, J., J. Boatwright, L. Haar, T. Hanks, and A. McGarr (1984). Source parameters for aftershocks of the Oroville, California, earthquake, *Bull. Seism. Soc. Am.* **74,** 1101–1123.

Hanks, T. C. (1977). Earthquake stress drops, ambient tectonic stresses and stresses that drive plate motions, *Pageoph* **115,** 441–458.

Hanks, T. C., and H. Kanamori (1979). A moment magnitude scale, *J. Geophys. Res.* **84,** 2348–2350.

Hanks, T. C., and R. K. McGuire (1981). The character of high-frequency strong ground motion, *Bull. Seism. Soc. Am.* **71,** 2071–2095.

Kanamori, H., and D. L. Anderson (1975). Theoretical basis of some empirical relations in seismology, *Bull. Seism. Soc. Am.* **65,** 1073–1095.

Kanamori, H., and T. H. Heaton (2000). Microscopic and macroscopic physics of earthquakes, in *GeoComplexity and the Physics of Earthquakes*, J. B. Rundle, D. L. Turcotte, and W. Klein (Editors), Geophysical Monograph 120, American Geophysical Union, Washington, DC, 147–163.

Kurushin, R. A., A. Bayasgalan, M. Olziybat, B. Enhtuvshin, P. Molnar, Ch. Bayarsayhan, K. W. Hudnut, and J. Lin (1997). The surface rupture of the 1957 Gobi-Altay, Mongolia, earthquake, Geol. Soc. Am. Spec. Paper 320, 143 pp.

Okal, E. A. (1976). A surface-wave investigation of the rupture mechanism of the Gobi-Altai (December 4, 1957) earthquake, *Phys. Earth Planet. Inter.* **12,** 319–328.

Romanowicz, B. (1992). Strike-slip earthquakes on quasi-vertical transcurrent faults: inferences for general scaling relations, *Geophys. Res. Lett.* **19,** 481–484.

Romanowicz, B. (1994). Comment on "A reappraisal of large earthquake scaling", *Bull. Seism. Soc. Am.* **84,** 1675–1676.

Romanowicz, B., and J. B. Rundle (1993). On scaling relations for large earthquakes, *Bull. Seism. Soc. Am.* **83,** 1294–1297.

Scholz, C. H. (1982). Scaling laws for large earthquakes: consequences for physical models, *Bull. Seism. Soc. Am.* **72,** 1–14.

Scholz, C. H. (1994a). A reappraisal of large earthquake scaling, *Bull. Seism. Soc. Am.* **84,** 215–218.

Scholz, C. H. (1994b). Reply to Comments on "A reappraisal of large earthquake scaling", *Bull. Seism. Soc. Am.* **84,** 1677–1678.

Scholz, C. H. (1997). Size distributions for large and small earthquakes, *Bull. Seism. Soc. Am.* **87,** 1074–1077.

Scholz, C. H., C. A. Aviles, and S. G. Wesnousky (1986). Scaling differences between large interplate and intraplate earthquakes, *Bull. Seism. Soc. Am.* **76,** 65–70.

Shaw, B. E., and C. H. Scholz (2001). Slip-length scaling in large earthquakes: observations and theory and implications for earthquake physics, *Geophys. Res. Lett.* **28,** 2995–2998.

Sieh, K. E. (1978). Slip along the San Andreas fault associated with the great 1857 earthquake, *Bull. Seism. Soc. Am.* **68,** 1421–1448.

Stein, R. S. and T. C. Hanks (1998). $\mathbf{M} \geq 6$ earthquakes in southern California during the twentieth century: no evidence for a seismicity or moment deficit, *Bull. Seism. Soc. Am.* **88,** 635–652.

Stein, R. S., A. A. Barka, and J. H. Dieterich (1997). Progressive failure on the North Anatolian fault since 1939 by earthquake stress triggering, *Geophys. J. Int.* **128,** 594–604.

Thatcher, W., and T. C. Hanks (1973). Source parameters of southern California earthquakes, *J. Geophys. Res.* **78,** 8547–8576.

Wells, D. L., and K. J. Coppersmith (1994). New empirical relationships among magnitude, rupture length, rupture width, rupture area, and surface displacement, *Bull. Seism. Soc. Am.* **84,** 974–1002.

Wyss, M. (1979). Estimating maximum expectable magnitude of earthquakes from fault dimensions, *Geology* 7, 336–340.

Zhang, W., D. Jiao, P. Zhang, P. Molnar, B. C. Burchfiel, Q. Deng, Y. Wang, and F. Song (1987). Displacement along the Haiyuan fault associated with the great 1920 Haiyuan, China, earthquake, *Bull. Seism. Soc. Am.* **77,** 117–131.

Robert E. Wallace Earthquake Center
U.S. Geological Survey, MS 977
345 Middlefield Road
Menlo Park, California 94025
thanks@usgs.gov

Manuscript received 15 April 2001.